Inositol hexakisphosphate kinase 3 promotes focal adhesion turnover via interactions with dynein intermediate chain 2

Tomas Rojas[a,1], Weiwei Cheng[b,1], Zhe Gao[c], Xiaoqi Liu[c], Yakun Wang[c], Adarsha P. Malla[a], Alfred C. Chin[a], Lewis H. Romer[d,e,f,g,h], Solomon H. Snyder[a,i,j,2], and Chenglai Fu[c,2]

[a]Solomon H. Snyder Department of Neuroscience, The Johns Hopkins University School of Medicine, Baltimore, MD 21205; [b]Division of Neuropathology, Department of Pathology, The Johns Hopkins University School of Medicine, Baltimore, MD 21205; [c]Department of Physiology and Pathophysiology, Tianjin Medical University, 300070 Tianjin, China; [d]Department of Anesthesiology and Critical Care Medicine, Johns Hopkins University, Baltimore, MD 21287; [e]Department of Cell Biology, Johns Hopkins University, Baltimore, MD, 21287; [f]Department of Biomedical Engineering, Johns Hopkins University, Baltimore, MD 21287; [g]Department of Pediatrics, Johns Hopkins University, Baltimore, MD 21287; [h]Center for Cell Dynamics, Johns Hopkins University, Baltimore, MD 21287; [i]Department of Pharmacology and Molecular Sciences, The Johns Hopkins University School of Medicine, Baltimore, MD 21205; and [j]Department of Psychiatry and Behavioral Sciences, The Johns Hopkins University School of Medicine, Baltimore, MD 21205

Contributed by Solomon H. Snyder, December 19, 2018 (sent for review October 9, 2018; reviewed by Per-Olof Berggren and Stephen B. Shears)

Cells express a family of three inositol hexakisphosphate kinases (IP6Ks). Although sharing the same enzymatic activity, individual IP6Ks mediate different cellular processes. Here we report that IP6K3 is enriched at the leading edge of migrating cells where it associates with dynein intermediate chain 2 (DIC2). Using immunofluorescence microscopy and total internal reflection fluorescence microscopy, we found that DIC2 and IP6K3 are recruited interdependently to the leading edge of migrating cells, where they function coordinately to enhance the turnover of focal adhesions. Deletion of IP6K3 causes defects in cell motility and neuronal dendritic growth, eventually leading to brain malformations. Our results reveal a mechanism whereby IP6K3 functions in coordination with DIC2 in a confined intracellular microenvironment to promote focal adhesion turnover.

IP6K | focal adhesion | dynein | cell migration | FAK

Cells express a family of three inositol hexakisphosphate kinases (IP6Ks), which generate 5-diphosphoinositol pentakisphosphate (5-IP7) by pyrophosphorylating inositol hexakisphosphate on the 5-position (1). In mammalian cells, 90% of total IP7 is 5-IP7 (2). Another form of IP7 is 1-IP7, which is produced by diphosphoinositol pentakisphosphate kinases (PPIP5Ks) acting at the 1-position of the inositol ring (3). PPIP5K also uses 5-IP7 to make bisdiphosphoinositol tetrakisphosphate (1,5PP-IP4 or IP8) (2). Reported functions of 5-IP7 include regulation of insulin release (4, 5), protein pyrophosphorylation (6), and energy metabolism (7). Although IP6Ks share the same kinase activity, their functions vary depending on the immediate intracellular microenvironment. IP6K1 regulates energy consumption (8), gene transcription (9), immune response (10), and male fertility (11, 12). IP6K2 physiologically mediates cell death (13–15). IP6K3 promotes synapse formation in cerebellar Purkinje cells (16), regulates lifespan (17), and plays a role in the onset of Alzheimer's disease (18).

Cytoplasmic dynein is a microtubule-based cytoskeleton motor that is responsible for retrograde movement of intracellular vesicles, organelles, and large protein and RNA-containing complexes (19). Dynein also functions at the cell membrane, where it tethers and/or generates pulling forces (20). Dynein is a complex composed of multiple subunits: heavy chain (DHC), intermediate chains (DIC), light intermediate chains (DLIC), and light chains (DLCs) (20). Dynein interacts with dynactin through binding between DIC and p150glued, a major subunit of dynactin (21). The interaction between DIC and p150glued is critical for dynein function (22). During cell migration, dynein is enriched at the leading edge (23), where it pulls the centrosome and the nucleus (24–26). Cytoplasmic dynein interacts with microtubules and some nonmicrotubule proteins at the cell membrane (23, 27) to regulate microtubule dynamics and centrosome reorientation in living cells (28). However, functions of dynein at the leading edge during cell migration have been elusive.

Focal adhesions are mediated by large dynamic multiprotein complexes whereby cells interact with the environment (29). Nascent focal adhesions (often called focal complexes) are initiated at the leading edge of cell protrusions. Focal adhesion turnover is restricted to protrusive regions of cells, although disassembly of focal adhesions occurs at the rear portion of cells (30). Focal adhesion assembly and disassembly and cell motility are mediated in part by focal adhesion kinase (FAK) activity (31–33). Deregulation of FAK is associated with defective focal adhesion dynamics and impairment of cell movement (34–36), yet spatial and temporal regulation of focal adhesions during coordinated and productive cell movement or migration remains incompletely understood.

In this study, we investigated cellular localization and functions of IP6K3. We found that IP6K3 is highly expressed at the leading edge of migrating cells. We observed a selective interaction of IP6K3 with dynein intermediate chain 2 (DIC2). IP6K3 and DIC2 are recruited interdependently to the leading edge of migrating cells, where they coordinately enhance the dynamics of focal adhesion. Deletion of IP6K3 leads to a major defect of focal adhesion dynamics. Consistently, deletion of

Significance

Cells express a family of three inositol hexakisphosphate kinases (IP6Ks), whose functions depend on the intracellular microenvironment. We find that IP6K3 is enriched at the migrating leading edge of cell membranes, where IP6K3 physiologically interacts with protein dynein intermediate chain 2 (DIC2). The cell membrane localizations of IP6K3 and DIC2 are interdependent. At the cell membrane, IP6K3 promotes cell motility via influences on the turnover of cell adhesions. Deletion of IP6K3 impairs neuronal cell migration and elicits brain malformation.

Author contributions: S.H.S. and C.F. designed research; T.R., W.C., Z.G., X.L., Y.W., A.P.M., A.C.C., and C.F. performed research; T.R., L.H.R., S.H.S., and C.F. analyzed data; and W.C., L.H.R., S.H.S., and C.F. wrote the paper.

Reviewers: P.-O.B., Karolinska Institutet; and S.B.S., National Institute of Environmental Health Sciences.

The authors declare no conflict of interest.

[1]T.R. and W.C. contributed equally to this work.

[2]To whom correspondence may be addressed. Email: ssnyder@jhmi.edu or chenglaifu@tmu.edu.cn.

This article contains supporting information online at www.pnas.org/lookup/suppl/doi:10.1073/pnas.1817001116/-/DCSupplemental.

Published online February 4, 2019.

IP6K3 disrupts neuronal cell motility and eventually causes brain malformation.

Results

IP6K3 Is at the Leading Edge of Migrating Cells. To understand diversity of IP6 kinases, we investigated their intracellular localizations. Mice brain and mouse embryonic fibroblast cells (MEFs) express all three IP6Ks (*SI Appendix*, Fig. S1*A*). We performed cell fractionation and found that IP6K3 and IP6K1 are enriched in the plasma membrane in both mice brain and MEFs, while IP6K2 is mainly in the nucleus (*SI Appendix*, Fig. S1 *B* and *C*). The cellular localizations of IP6Ks are confirmed by immunostaining of IP6Ks in cortical neurons (*SI Appendix*, Fig. S1*D*) and MEFs (*SI Appendix*, Fig. S1*E*). The human neuroblastoma SH-SY5Y cells also express three IP6Ks (*SI Appendix*, Fig. S2*A*). We performed total internal reflection fluorescence (TIRF) microscopy, which illustrates only ∼100 nm above the coverslip to achieve high signal-to-noise ratios (*SI Appendix*, Fig. S2*B*). IP6K3 is seen at the leading edge of migrating SH-SY5Y cells in a wound-induced migration assay (*SI Appendix*, Fig. S2*B*). IP6K3 also occurs at membrane protrusions in apparently migrating MEFs observed by immunofluorescence microscopy (*SI Appendix*, Fig. S2 *C–F*). To further explore the intracellular localization of IP6K3, we immunostained IP6K3 together with markers for the Golgi apparatus (*SI Appendix*, Fig. S2*D*), mitochondria (*SI Appendix*, Fig. S2*E*), or lysosome (*SI Appendix*, Fig. S2*F*). IP6K3 does not apparently localize in any of those organelles.

IP6K3 Interacts with Dynein Intermediate Chain 2. We wondered whether the functions of IP6K3 are reflected by its associated proteins. We immunoprecipitated IP6K3 and searched for binding partners. Several proteins pulled down by IP6K3 from the wild-type tissues are lost in the *IP6K3* knockouts (Fig. 1*A*). Presumably the missing bands in the KOs reflect proteins that physiologically associate with IP6K3. One of the prominent bands is identified as dynein intermediate chain 2 (DIC2) (Fig. 1*A*). We confirmed IP6K3/DIC2 interaction by immunoprecipitation of IP6K3 or DIC2, which reveals binding of IP6K3/DIC2 in WT preparations but not in the *IP6K3* knockouts (Fig. 1*B*). To rule out nonspecific activity of the IP6K3 antibody, we expressed flag-tagged IP6K3 and myc-tagged DIC2 in human embryonic kidney (HEK) 293 cells and validated the IP6K3/DIC2 binding by immunoprecipitation of flag tag and myc tag (Fig. 1 *C* and *D*). IP6K3 binds robustly to DIC2 in vitro as does the kinase-deficient IP6K3 (K217A) (*SI Appendix*, Fig. S3). Thus, the catalytic activity of IP6K3 is not required for its binding with DIC2. DIC2 binds specifically to IP6K3, because immunoprecipitation of either IP6K1 or IP6K2 does not pull down DIC2 (Fig. 1 *E* and *F*). Consistently, immunoprecipitation of DIC2 pulls down IP6K3 but not IP6K1 or IP6K2 (Fig. 1*G*). We aligned IP6Ks' protein sequences using the web services provided by the European Molecular Biology Laboratory-European Bioinformatics Institute (EMBL-EBI) (37). The amino acid sequences of substrate binding regions of IP6Ks are identical. The amino acid sequence of IP6K3 kinase domain displays ∼70% identity to that of IP6K1 and IP6K2; however, the variable regions of IP6Ks are less than 20% identical (*SI Appendix*, Fig. S2). Thus, the distinct intracellular localizations and functions of IP6Ks may be determined by their variable regions. DIC2 binds to the 67- to 138-amino acid fragment of IP6K3, which is unique to IP6K3 (Fig. 1 *H–J*).

Recruitment of DIC2 to the Leading Edge Requires IP6K3. Deletion of IP6K3 does not affect the expression levels of dynein heavy chain (DHC), intermediate chain 1 (DIC1), intermediate chain 2 (DIC2), light intermediate chain 1 (DLIC1), light chain (DLC), and the dynactin subunit p150glued (Fig. 2*A*). The binding between IP6K3 and DIC2 is specific, because immunoprecipitation of IP6K3 does not pull down DHC, DIC1, DLIC1, DLC, or p150glued (Fig. 2*B*). Bhandari and coworkers have reported that depletion of 5-IP7 weakens the interaction of DICs/p150glued (38). We thus wondered whether knockout of IP6K3 affects the interaction between DIC2 and p150glued. Indeed, immunoprecipitation of DIC2 pulls down substantially less p150glued from the *IP6K3* KOs (Fig. 2*C*). In contrast, equal amounts of p150glued are pulled down by DIC1 from *IP6K3* WTs and KOs (Fig. 2*D*). Consistently, immunoprecipitation of p150glued in the *IP6K3* KO brain tissues pulls down significantly less DIC2 but equal amounts of DIC1 (Fig. 2*E*). Thus, IP6K3 is required for DIC2/p150glued interaction.

The interaction of DIC with p150glued mediates the recruitment of dynein to the cell membrane (39, 40). We thus investigated whether deletion of IP6K3 influences DIC2 at the cell membrane. Indeed, DIC2 levels in the plasma membrane fraction are notably reduced in *IP6K3* KO MEFs (Fig. 2*F*). Immunostaining of DIC2 on *IP6K3* KO MEFs shows diminished DIC2 at the cell membranes (Fig. 2*G*). In a wound-induced migration assay, recruitment of DIC2 to the leading edge is substantially decreased in *IP6K3* knockout MEFs (Fig. 2*H*). We isolated mouse astrocytes (*SI Appendix*, Fig. S4). Deletion of IP6K3 in astrocytes reduces IP7 by 25% (*SI Appendix*, Fig. S4). We performed TIRF microscopy on a wound-induced migration assay of astrocytes (Fig. 2*I*). Deletion of IP6K3 abolishes the recruitment of DIC2 to the leading edge (Fig. 2*I*). Immunostaining of pericentrin for centrosomes in a wound-induced migration assay reveals disruption of centrosome orientation in *IP6K3* KO MEFs (centrosomes are orientated in 75% WT cells vs. 40% in *IP6K3* KO cells), consistent with the deficit of DIC2 at the leading edge (41) (Fig. 2*J*). Centrosome orientation is defined as the centrosome occurring between the nucleus and the wound edge (±45° deviation from the direction perpendicular to the wound) (41).

IP6K3 Promotes Focal Adhesion Dynamics in the Leading Edge. To further explore the influence of IP6K3 upon DIC2, we blotted for phosphoserine/threonine and phosphotyrosine in the DIC2 immunoprecipitations from *IP6K3* WT and KO brain tissues (Fig. 3*A*). A phosphotyrosine band with molecular weight around 120 kDa occurs in the WT but not the *IP6K3* KO preparations (Fig. 3*A*). This result is reminiscent of FAK, whose phosphorylation is enhanced by 5-IP7 (42, 43). We thus investigated FAK phosphorylation in *IP6K3* KO brain tissues. Levels of phosphorylated FAK are moderately decreased in the *IP6K3* KO tissues, as is phosphorylated paxillin (Fig. 3*B*). Immunoprecipitation of DIC2 pulls down much less phosphorylated FAK in the *IP6K3* KOs (Fig. 3*C*), although there is no difference in total FAK. IP6K3 does not associate with FAK or paxillin directly (*SI Appendix*, Fig. S5). We immunostained phosphorylated FAK (Y397) in *IP6K3* WT and KO astrocytes. Density of phosphorylated FAK at the cell peripheral is markedly decreased in IP6K3-deleted cells (Fig. 3 *D* and *G*). Similarly, the density of phosphorylated paxillin, which is the target of FAK, is also decreased in the *IP6K3* KO astrocytes (Fig. 3 *E* and *H*). The sizes of focal adhesions at the cell cortex of the *IP6K3* KO astrocytes are relatively larger, revealed by vinculin staining, indicating fewer turnovers of focal adhesions (Fig. 3 *F–H*). We also immunostained phosphorylated FAK (Y397) and phosphorylated paxillin and vinculin in a wound-induced migration assay. Deletion of IP6K3 greatly decreases phosphorylation of FAK (Fig. 3*I*) and paxillin (Fig. 3*J*) at the leading edge of migrating cells. Vinculin stains tiny spots at the leading edge of *IP6K3* KO astrocytes, which is consistent with the concept that the recruitment of vinculin to focal adhesions requires FAK-mediated paxillin phosphorylation (44). Thus, deletion of IP6K3 elicits deficits of focal adhesion maturation (Fig. 3*K*). Defective actin filament assembly at the leading edge is also

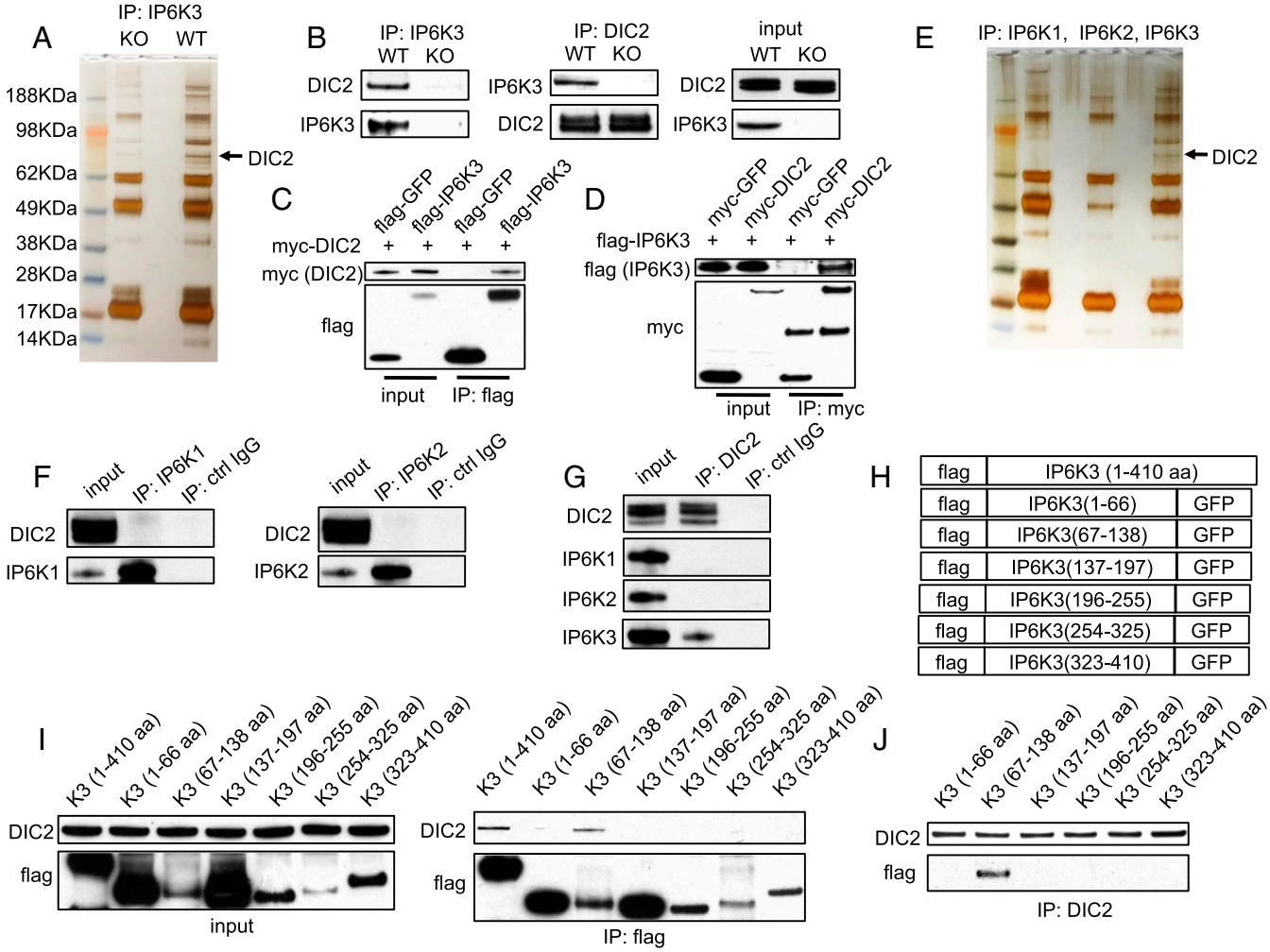

Fig. 1. IP6K3 physiologically associates with DIC2. (*A*) Immunoprecipitation of IP6K3 from WT and *IP6K3* KO mice brain tissues, silver staining, and mass spectrometry-identified DIC2 is pulled down by antibodies against IP6K3. (*B*) Immunoprecipitation of IP6K3 or DIC2 from WT and *IP6K3* KO brains; Western blot shows IP6K3 binds with DIC2. (*C*) Flag-GFP or flag-IP6K3 was overexpressed together with myc-DIC2 in HEK 293 cells; immunoprecipitation of flag (IP6K3) pulls down myc (DIC2). Flag-GFP is a negative control. (*D*) Myc-GFP or myc-DIC2 was overexpressed together with flag-IP6K3 in HEK 293 cells; immunoprecipitation of myc (DIC2) pulls down flag (IP6K3). Myc-GFP is a negative control. (*E*) Immunoprecipitation of IP6K1, IP6K2, and IP6K3 from WT mice brain tissues. Silver staining shows DIC2 is specifically pulled down by IP6K3. (*F*) Immunoprecipitation of IP6K1 and IP6K2 from WT mice brain tissues. Western blot shows DIC2 is not coprecipitated by IP6K1 or IP6K2. (*G*) Immunoprecipitation of DIC2 or control IgG from WT mice brains. Western blot reveals DIC2 pulls down IP6K3 but not IP6K1 or IP6K2. (*H*) Schematic representation of flag-tagged IP6K3 fragments used in the binding studies in *I* and *J*. (*I*) Immunoprecipitation of flag (IP6K3 fragments); Western blot shows DIC2 is pulled down by the 67- to 138-amino acid fragment of IP6K3. (*J*) Immunoprecipitation of DIC2; Western blot shows DIC2 specifically interacts with the 67- to 138-amino acid fragment of IP6K3.

evident in IP6K3-deleted astrocytes (Fig. 3 *I–K*). Thus, IP6K3 is required for focal adhesion dynamics in the leading edge.

DIC2 Takes IP6K3 to the Leading Edge to Promote Focal Adhesion Turnover. To test whether DIC2 is responsible for the recruitment of IP6K3 to the leading edge, we depleted DIC2 in human neuroblastoma SH-SY5Y cells by shRNA transduction (Fig. 4*A*) and observed the intracellular localization of IP6K3 by immunofluorescence microscopy (Fig. 4*B*). Knocking down DIC2 substantially decreases the amount of IP6K3 at the cell leading edge (Fig. 4*B*). TIRF microscopy reveals polarized intracellular localizations of IP6K3 with a substantial amount at the cell membrane (Fig. 4*C*). In striking contrast, in the DIC2-deleted cells, IP6K3 is mainly in the cytosol and accumulated around the nucleus without polarized distribution (Fig. 4 *B* and *C*). In the wound-induced migration assay, deletion of DIC2 significantly reduces recruitment of IP6K3 to the leading edge, demonstrated by TIRF microscopy (Fig. 4*D*). Thus, DIC2 is required for the recruitment of IP6K3 to cell membranes.

We asked whether disrupted IP6K3's plasma membrane localization affects FAK phosphorylation in DIC2-deleted cells. Knocking down DIC2 substantially diminishes the density of phospho-FAK in cell membranes (Fig. 4 *E* and *G*). Similarly, depletion of DIC2 results in a dramatic diminution of phosphopaxillin at the cell protrusion region (Fig. 4 *F* and *H*). Thus, DIC2 drives IP6K3 to the migrating leading edge to promote the turnover of focal adhesions.

Deletion of IP6K3 Causes Defects in Neuronal Cell Migration and Brain Malformation. To characterize IP6K3/DIC2/FAK activities in a more physiological setting, we isolated mouse primary cortical neurons and investigated the influence of IP6K3 upon dendritic growth. Deletion of IP6K3 leads to a markedly reduced length of neuronal processes (Fig. 5*A*). This phenotype is rescued by WT IP6K3 but not the kinase-deficient mutant (Fig. 5*B*). Consistently,

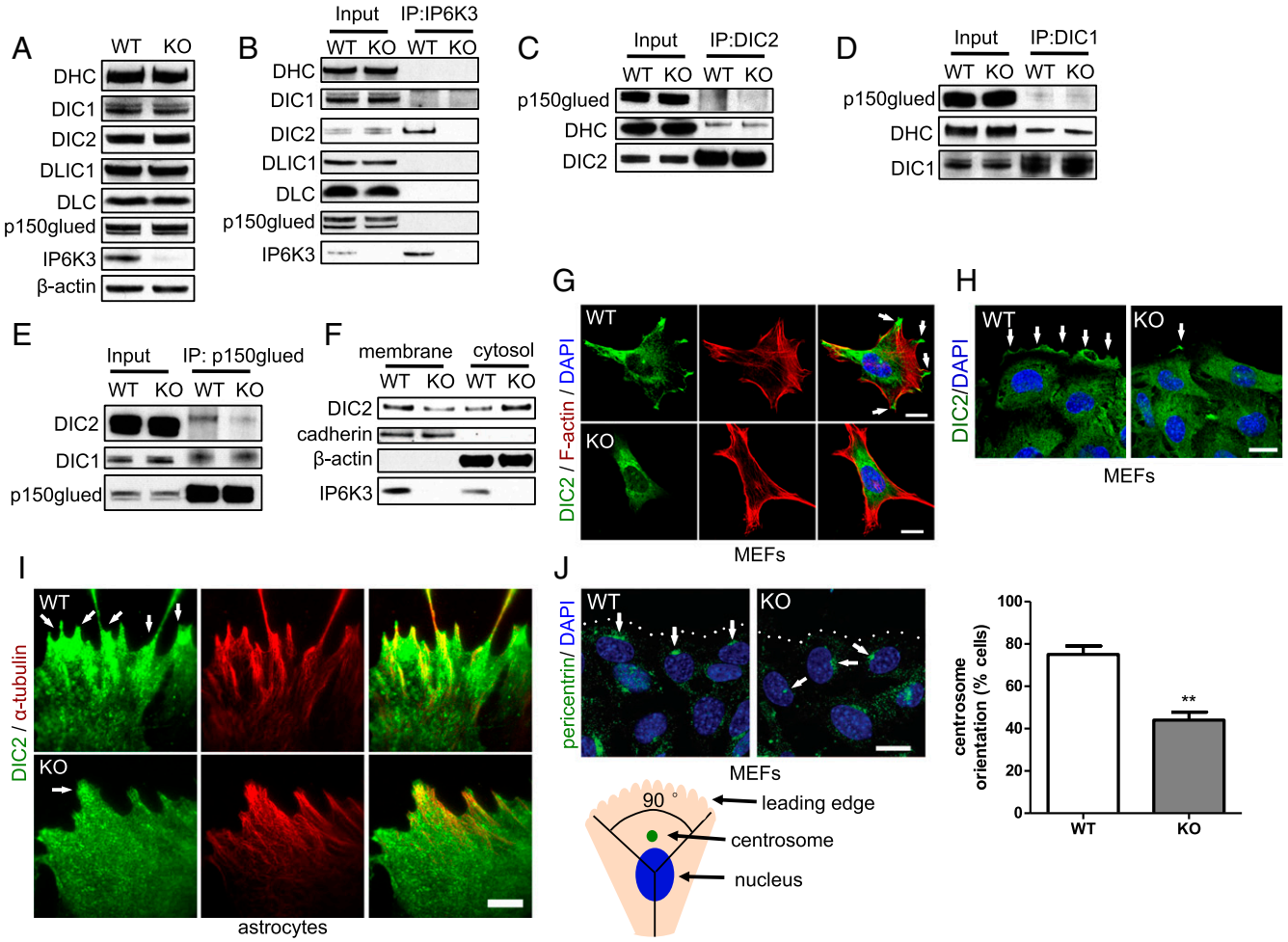

Fig. 2. Recruitment of DIC2 to the leading edge requires IP6K3. (*A*) Western blot shows that the expression levels of DHC, DIC1, DIC2, DLIC1, DLC, and p150glued do not change in the *IP6K3* KO brains. (*B*) Immunoprecipitation of IP6K3 from WT and *IP6K3* KO brains; Western blot reveals IP6K3 binds only with DIC2 but not the other subunits of the dynein complex. (*C*) Immunoprecipitation of DIC2 from WT and *IP6K3* KO brains; substantially less p150glued is pulled down by DIC2 from the *IP6K3* KOs. (*D*) Immunoprecipitation of DIC1 from WT and *IP6K3* KO brains; equal amounts of p150glued are pulled down by DIC1. (*E*) Immunoprecipitation of p150glued from WT and *IP6K3* KO brains. Much less DIC2 is pulled down by p150glued in the *IP6K3* KOs, whereas no difference is evident for DIC1. (*F*) Subcellular fractionation of MEFs; deletion of IP6K3 dramatically decreases DIC2 in the cell membrane fraction. (*G*) Immunostaining of DIC2 in WT and *IP6K3* KO MEFs; IP6K3 deletion disrupts DIC2 membrane localization (arrows point to DIC2 on the cell membrane in WTs) (Scale bar: 20 μm.) (*H*) Immunostaining of DIC2 in MEFs in a wound-induced migration assay; the leading edge recruitment of DIC2 is disrupted in *IP6K3* KO MEFs (arrows point to DIC2 at the leading edge). (Scale bar: 20 μm.) (*I*) Immunostaining of DIC2 in astrocytes in a wound-induced migration assay; recruitment of DIC2 to the leading edge is disrupted in *IP6K3* KO astrocytes, as revealed by TIRF microscopy (arrows point to DIC2 at the leading edge). (Scale bar: 5 μm.) (*J*) Immunostaining of pericentrin for centrosome (arrows) in MEFs in a wound-induced migration assay. Centrosome orientation is defined as positioning of the centrosome between the nucleus and the wound edge (±45° deviation from the direction perpendicular to the wound). Dotted line shows migrating leading edge observed in bright field. $^{**}P < 0.01$. (Scale bar: 20 μm.)

the *IP6K3* KO Purkinje cells display dendritic growth retardation (Fig. 5*C*). We evaluated the IP6K3/DIC2/FAK activities in several models of cell migration. In a scratch assay in MEFs, deletion of IP6K3 causes a 40% decrease in movement (*SI Appendix*, Fig. S6*A*). The Boyden chamber assay shows a 50% decline of migration in the *IP6K3* KO preparations (*SI Appendix*, Fig. S6*B*). We rescued the protein expression in *IP6K3* knockout MEFs by overexpressing WT IP6K3 or catalytically inactive IP6K3-kinase dead (KD) (*SI Appendix*, Fig. S6*C*). In both the scratch assay (*SI Appendix*, Fig. S6*D*) and the Boyden chamber assay (*SI Appendix*, Fig. S6*E*), the defect of *IP6K3* knockouts in motility is reversed by WT IP6K3 but not by the catalytically dead mutant.

To test whether IP6K3 deletion impairs neuronal cell migration, we monitored neuronal disposition at embryonic day 15.5 (E15.5) following the administration of 5-ethynyl-2′-deoxyuridine (EdU) (Fig. 5 *D* and *E*). Retardation of neuronal migration is evident in *IP6K3* mutants at 24 h after EdU administration and persists at 48 h.

We evaluated the neuronal movement of different cortical layers by staining endogenous Satb2 and Ctip2 for layers 2–4 and 5, respectively (Fig. 5*F* and *SI Appendix*, Fig. S7*A*). At E15.5 a large number of Satb2-positive cells have migrated to the superficial layers in the WTs; however, sparse Satb2 positive cells are evident in the superficial layer in the *IP6K3* KOs (Fig. 5*F*). Consistently, at E17.5 Satb2- and Ctip2-positive neurons appear to have attained their adult sites in the WTs, whereas in the *IP6K3* knockouts, migration of Satb2 and Ctip2 continues (*SI Appendix*, Fig. S7*A*).

We stained calbindin for Purkinje cells in the cerebellum and monitored their movement during development. At E19.5, the WT Purkinje cells have completed migration to the cerebellar cortex, whereas, the *IP6K3* KO Purkinje cells are still migrating

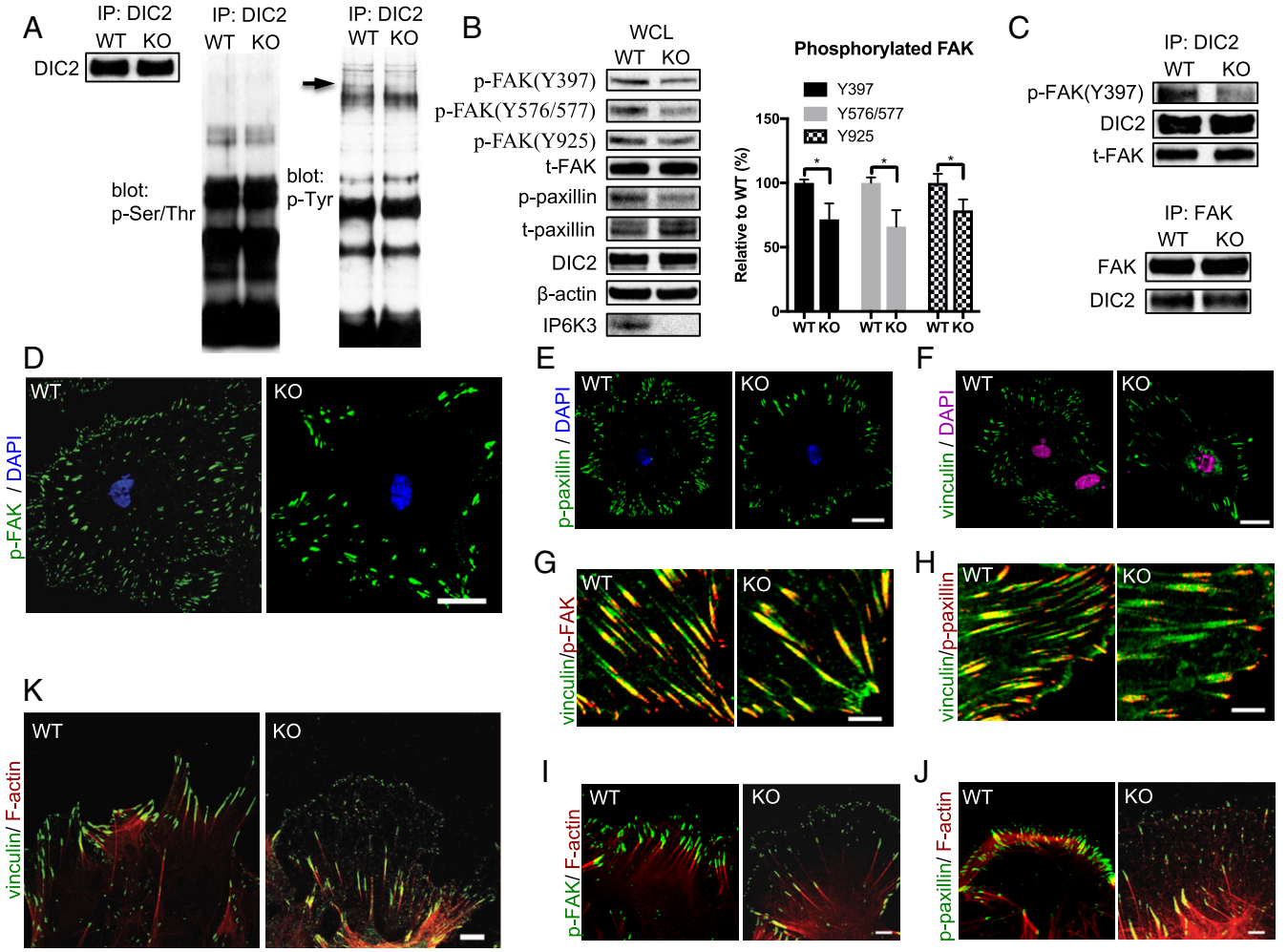

Fig. 3. IP6K3 promotes focal adhesion dynamics in the leading edge. (*A*) Immunoprecipitation of DIC2 from *IP6K3* WT and KO brains then blotted to examine phosphoserine/threonine and phosphotyrosine; a phosphotyrosine band at molecular weight around 120 kDa (arrow) is missing in the *IP6K3* KO preparations. (*B*) Western blot shows moderate decrease of phospho-FAK and phosphopaxillin in the whole cell lysates of *IP6K3* KO brains. **P* < 0.05. (*C*) Immunoprecipitation of DIC2 and FAK from *IP6K3* WT and KO brains; Western blot reveals DIC2 pulls down much less phosphorylated FAK in *IP6K3* KOs, although there is no difference in total FAK. (*D*) Immunostaining of phospho-FAK (Y397) in astrocytes; deletion of IP6K3 elicits a substantially reduced density of phospho-FAK at the cell periphery. (Scale bar: 20 μm.) (*E*) Immunostaining of phosphopaxillin in astrocytes; deletion of IP6K3 elicits a markedly diminished density of phosphopaxillin at the cell periphery. (Scale bar: 20 μm.) (*F*) Immunostaining of vinculin reveals a larger size of focal adhesions at the cell periphery of the *IP6K3* KO astrocytes. (Scale bar: 20 μm.) (*G*) Immunostaining of vinculin and phospho-FAK (Y397) in astrocytes. At the cell periphery of *IP6K3* KO astrocytes, the focal adhesion sizes are larger and the density of phospho-FAK is substantially decreased. (Scale bar: 5 μm.) (*H*) Immunostaining of vinculin and phosphopaxillin in astrocytes. At the cell periphery of *IP6K3* KO astrocytes, the focal adhesion sizes are larger and the density of phosphopaxillin is substantially decreased. (Scale bar: 5 μm.) (*I–K*) Wound induced astrocytes migration assay. (*I*) Immunostaining of phospho-FAK (Y397) and F-actin; the phospho-FAK is substantially decreased at the leading edge of *IP6K3* KO astrocytes. (Scale bar: 5 μm.) (*J*) Immunostaining of phosphopaxillin and F-actin; the phosphopaxillin is substantially decreased at the leading edge of *IP6K3* KO astrocytes. (Scale bar: 5 μm.) (*K*) Immunostaining of vinculin and F-actin; in the WTs, obvious focal adhesions (vinculin staining) that are linked with actin filaments are at the leading edge, whereas in the *IP6K3* KO astrocytes, the vinculin staining is less prominent and the spots are tiny at the leading edge. This may indicate delayed or less robust focal adhesion maturation. (Scale bar: 5 μm.) (*I–K*) Deletion of IP6K3 decreases actin assembly at the leading edge.

(Fig. 5*G*). At postnatal day 1 (P1), all of the WT Purkinje cells have reached the Purkinje cell layer, however, a number of *IP6K3* mutant cells are in the granule cell layer, indicating that they have not migrated to their mature position (Fig. 5*H*). At P7, the majority of *IP6K3* KO Purkinje cells have reached the Purkinje cell layer, but some are observed in the granule cell layer (Fig. 5*I*). This phenotype continues at P28 (Fig. 5*J*). Deletion of IP6K3 elicits cerebellar malformation, which presumably is the result of migration deficits (Fig. 5 *K* and *L* and *SI Appendix*, Fig. S7 *B* and *C*). The malformation is first observed at P7, when a number of Purkinje cells are trapped in the granule cell layer (Fig. 5*K* and *SI Appendix*, Fig. S7*B*), and lasts through adult life (Fig. 5*L* and *SI Appendix*, Fig. S7*C*).

Discussion

In this study, we investigated the intracellular localization and corresponding functions of IP6K3. IP6K3 displays a polarized intracellular distribution and is highly enriched in the leading edge of migrating cells, although not specifically to focal adhesion sites. IP6K3 physiologically associates with DIC2. IP6K3 and DIC2 are recruited together to the leading cell membranes. IP6K3 enhances the recruitment of DIC2 to the leading edge by promoting DIC2/p150glued interactions. Consequently, DIC2 takes IP6K3 to the cell membrane. At the cell membrane, IP6K3 promotes the phosphorylation of FAK and turnover of focal adhesions. Deletion of IP6K3 elicits defects of cell motility and brain malformation. Thus, our study reveals a

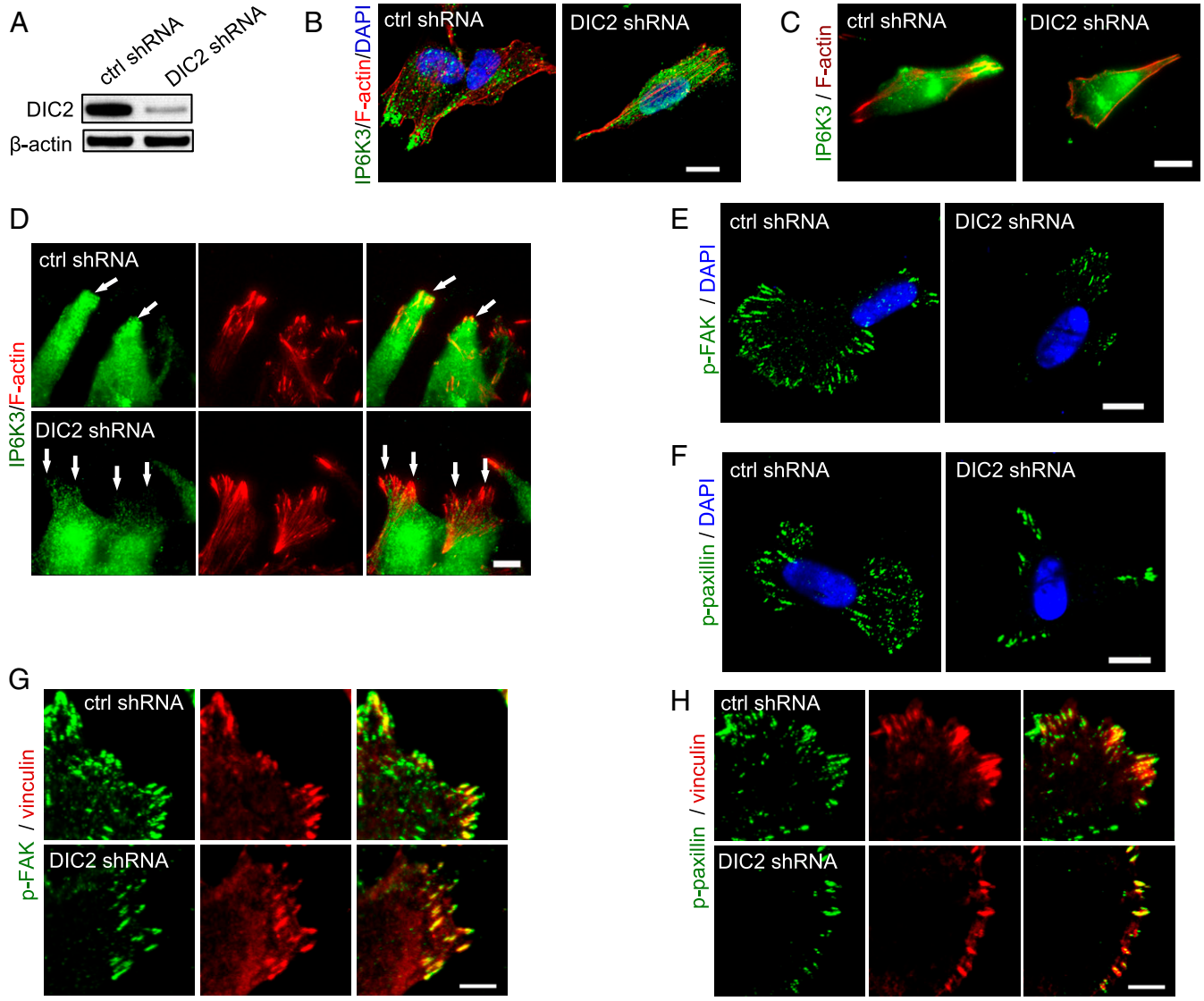

Fig. 4. DIC2 drives IP6K3 to the leading edge. (*A*) Knocking down DIC2 in human neuroblastoma SH-SY5Y cells by shRNA transduction. (*B–D*) Immunostaining of IP6K3 in SH-SY5Y cells. (*B*) DIC2 knockdown disrupts the plasma membrane localization of IP6K3. (Scale bar: 10 μm.) (*C*) TIRF microscopy reveals polarized intracellular distribution of IP6K3, which is enriched at the cell's leading edge in control cells. Deletion of DIC2 disrupts IP6K3 distribution. (Scale bar: 10 μm.) (*D*) TIRF microscopy demonstrates deletion of DIC2 abolishes the recruitment of IP6K3 to the leading edge in a wound-induced migration assay. (Arrows point to the leading edge.) (Scale bar: 5 μm.) (*E*) Immunofluorescence microscopy shows decreased density of phospho-FAK (Y397) at cell periphery in DIC2 knocked-down SH-SY5Y cells. (Scale bar: 10 μm.) (*F*) Immunofluorescence microscopy demonstrates decreased density of phosphopaxillin at the cell periphery in DIC2-deleted SH-SY5Y cells. (Scale bar: 10 μm.) (*G*) High magnification shows at the cell periphery the density of phospho-FAK (Y397) is dramatically decreased in DIC2 knocked-down SH-SY5Y cells. (Scale bar: 5 μm.) (*H*) High magnification shows at the cell periphery the density of phosphopaxillin is substantially decreased in DIC2 knocked-down SH-SY5Y cells. (Scale bar: 5 μm.)

mechanism by which IP6K3 and DIC2 coordinately regulate the dynamics of focal adhesion (Fig. 6).

Inositol pyrophosphates have been associated with FAK activity. IP6K1 generates 5-IP7 to promote FAK phosphorylation (42, 43). IP6K2, via its product 5-IP7, sequesters the tumor suppressor enzyme liver kinase B1 in the nucleus, thus blocking its repressive effects on FAK activity (45). In this study, we found IP6K3 is taken by DIC2 to the leading cell membranes, where it promotes FAK phosphorylation. In MEF cells, IP6K1 is responsible for up to 60% IP7 production (46). Thus, deletion of IP6K1 leads to a major defect of FAK phosphorylation (42, 43). Whereas IP6K3 generates less than 25% of cellular IP7 in astrocytes (this study), its enhancement of FAK phosphorylation in cell membranes supports the possibility that IP6K3 performs subtle functions in a specific intracellular microenviroment. Inositol pyrophosphates that are generated by IP6K1 promote dynein-mediated transportation (38). Dynein is responsible for transportation of the Golgi apparatus (47) and lysosome (48). However, IP6K3 does not apparently associate with those organelles, indicating IP6K3 may not influence dynein transportation, which is different from IP6K1 (38).

During cell migration, dynein is enriched in the leading cell membranes (23, 27), where it pulls the centrosome forward (49). Recruitment of dynein to the cell membrane is mediated by p150glued-dependent and -independent mechanisms (50). The 5-IP7 enhances the binding between DIC and p150glued (38). Deletion of IP6K3 depletes 5-IP7 in areas where IP6K3 is normally localized, thereby weakening the interaction of DIC2/p150glued, and consequently disrupting the recruitment of DIC2 to the cell membrane (40). However, the exact mechanisms

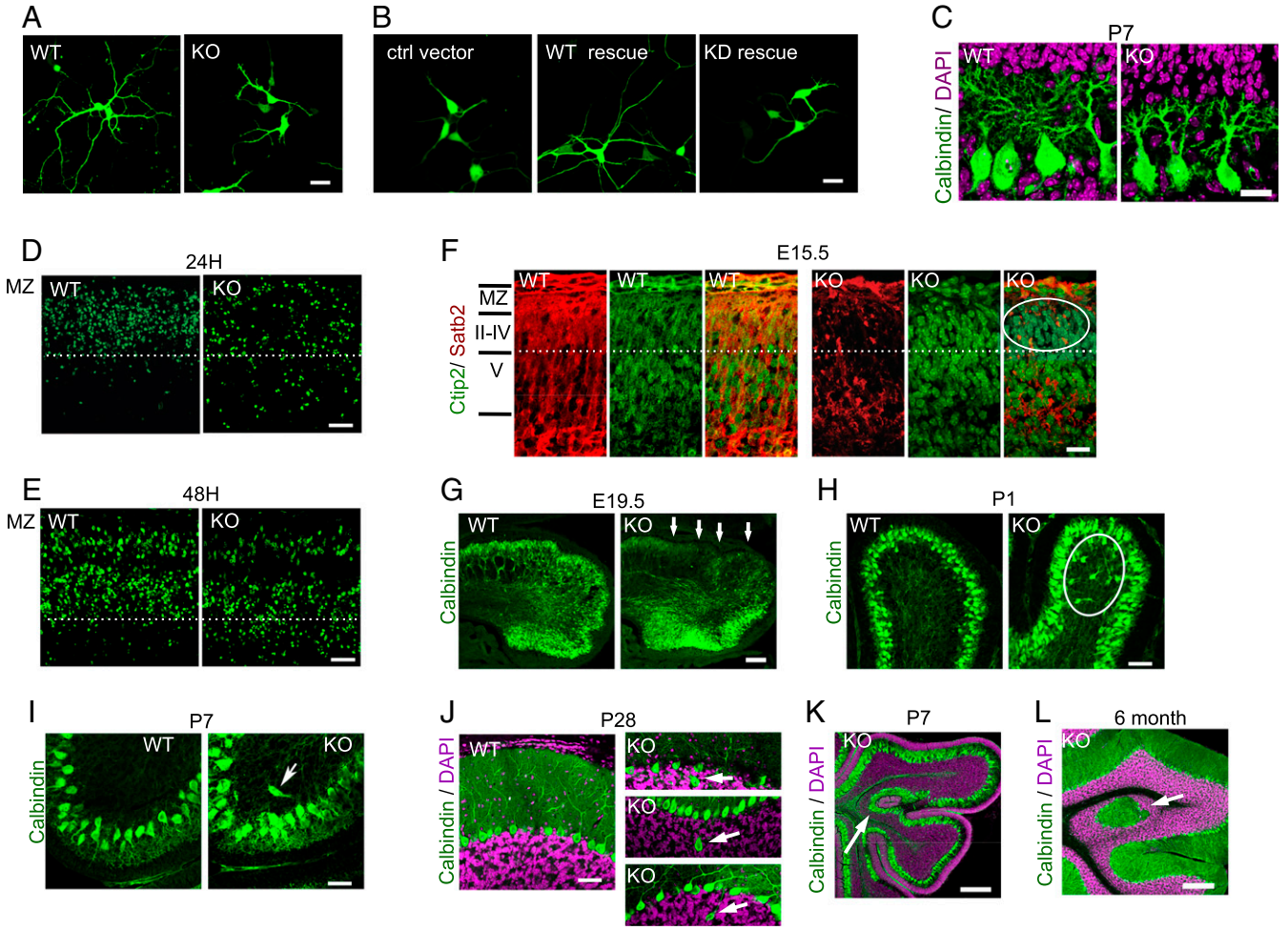

Fig. 5. IP6K3 deletion causes neuronal cell migration defects and brain malformation. (*A*) IP6K3 deletion impairs dendritic growth of cortical neurons. Neurons were labeled with GFP lentivirus and cultured in vitro for 5 d before images were taken. (Scale bar: 20 μm.) (*B*) IP6K3 KO neurons were rescued by lentiviral transduction of WT or kinase deficient (KD) IP6K3. Dendritic growth is rescued by WT IP6K3. (Scale bar: 20 μm.) (*C*) IP6K3 deletion elicits dendritic growth retardation in Purkinje cells. Image represents P7. Calbindin is immunostained for Purkinje cells. (Scale bar: 20 μm.) $n = 4$. (*D* and *E*) EdU was injected into pregnant heterozygous mice at E15.5; brain slices of the littermate fetuses were processed 24 and 48 h later. Substantially fewer EdU-positive cells migrate to the superficial layers of the *IP6K3* KOs at 24 h (*D*) and 48 h (*E*). (Scale bar: 50 μm.) $n = 4$. (*F*) Littermates of WT and *IP6K3* KO fetus brains (E15.5) were cut sagittally and stained with Satb2 for layers 2–4 and Ctip2 for layer 5. A number of WT Satb2-positive neurons have migrated to the top layers, whereas sparse *IP6K3* KO Satb2 neurons are in the top layers (circled area). (Scale bar: 20 μm.) $n = 3$. (*G–J*) Immunostaining calbindin for Purkinje cells in WT and *IP6K3* KO cerebellum. (*G*) At E19.5, Purkinje cells have reached and lined up in the cerebellar cortex in the WTs. In *IP6K3* KOs, Purkinje cells migrate only to 1/2 of the cerebellar cortex (arrows point to areas missing Purkinje cells in the KOs). (Scale bar: 100 μm.) $n = 3$. (*H*) At P1, all of the WT Purkinje cells have reached the Purkinje cell layer, whereas a number of the *IP6K3* KO cells remain in the migratory process (circle). (Scale bar: 50 μm.) $n = 3$. (*I*) At P7, some *IP6K3* KO Purkinje cells are still migrating to the Purkinje layer (arrow). (Scale bar: 50 μm.) $n = 3$. (*J*) At P28, some *IP6K3* KO Purkinje cells have not reached the Purkinje layer (arrow). A total of 20 separate fields were examined in each animal. (Scale bar: 50 μm.) $n = 3$. (*K* and *L*) Purkinje cells were immunostained by anticalbindin antibody. Nucleus was stained with DAPI. (*K*) At P7, a group of Purkinje cells is trapped in the granule layers (arrow) in the *IP6K3* KOs. (Scale bar: 100 μm.) $n = 3$. (*L*) Obvious brain malformation with a group of Purkinje cells in the granule layers (arrow) is evident in 6-mo-old *IP6K3* KOs. (Scale bar: 200 μm.) $n = 3$.

that recruit IP6K3 and DIC2 to the cell membrane have been elusive.

At the cell membrane, dynein is in adherens junctions (51) and focal adhesions (52). DIC2 binds with FAK, an interaction increases during cell migration (52). DIC2 is required for the turnover of focal adhesions at cell membranes (52); however, regulatory mechanisms have been elusive. We found that DIC2 takes IP6K3 to the cell membrane to promote FAK activity and the turnover of focal adhesions. FAK also occurs in centrosome where phosphorylation of FAK at serine 732 renders its interaction with DIC (53). The 5-IP7, the major product of IP6Ks, enhances FAK activity via increasing its phosphorylation at tyrosine 397 (42, 43). Consistently, deletion of IP6K3 decreases FAK phosphorylation at tyrosine 397. However, IP6K3 deletion does not alter the interaction between FAK and DIC2, indicating IP6K3 does not affect FAK phosphorylation at serine 732, which is mainly regulated by CDK5 (54).

Mutations in dynein or its regulators are linked to neurodevelopmental and neurodegenerative diseases (50). Deletion of IP6K3 also elicits brain malformation, albeit less severe than that of dynein mutants (55). Dendritic growth depends on normal FAK (56) and dynein functions (27). Deletion of IP6K3 disrupts DIC2 membrane localization and FAK activity thus delays the growth of neuronal processes. Disrupting the interaction between dynein and dynactin by inducing dynactin disassembly causes late-onset progressive motor neuron degenerative disease (57). IP6K3 contributes to late onset Alzheimer's disease (18). IP6K3 directly associates with DIC2. Inositol pyrophosphates

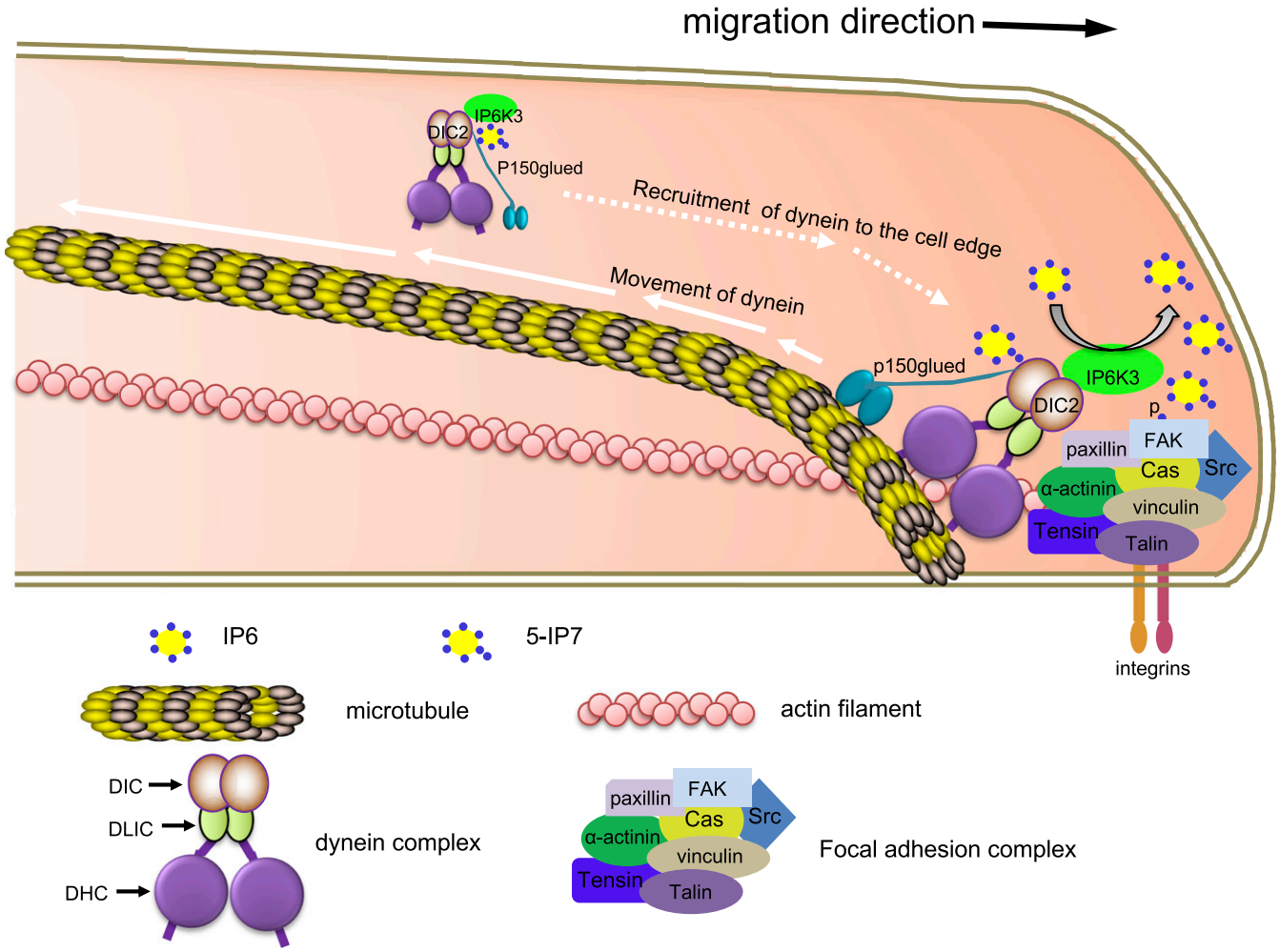

Fig. 6. Schematic image represents the mechanism by which IP6K3 and DIC2 promote focal adhesion dynamics coordinately. Dynein complex moves along the microtubule from cell edge to the center (centripetally) before it is recruited back to the cell edge. IP6K3 interacts with DIC2 and they are recruited together to the leading edge, where IP6K3 enhances the turnover of focal adhesions.

generated by IP6K3 enhances the interaction between DIC2 and p150glued, a major subunit of dynactin. Mutations in the promoter region of IP6K3 that increase its transcription activity are associated with a lower risk of late-onset Alzheimer's disease (18). Thus, the protective effects of elevated IP6K3 protein and 5-IP7 levels may involve regulation of dynein and FAK activities. Inositol pyrophosphates generated by IP6K1 also enhances the binding of DIC/p150glued, although no direct interaction has been found between IP6K1 and DIC (38). We previously found that deletion of IP6K1 induces brain malformation (42). The deficits of DIC/p150glued interaction in IP6K1 mutants may also contribute to the developmental defects. Earlier, we found that IP6K3 affects the morphology and synapse formation of cerebellar Purkinje cells (16). The IP6K3 deletion-induced brain malformation may also contribute to the deficits in motor learning and coordination (16). In our previous study, we did not anticipate alterations in brain structure. Accordingly, we focused on the midline of brain, which is the most common area to be investigated (16). The aberrant aggregations of Purkinje cells, however, occur in the lateral cerebellar hemispheres but not the midline vermis, and so were not detected.

Though IP6K3 produces only a small pool of 5-IP7, it performs critical cellular functions. Thus, 5-IP7 is not equally distributed in a cell. Individual pools of IP6K-generated 5-IP7 function in localized areas where the protein is concentrated. Discretely localized generation of 5-IP7 to maintain normal cell function may be the reason for a cell to express three IP6Ks. Differences in localization, expression, and kinase activity of the three isoforms may contribute to selective regulation of 5-IP7 generation.

Materials and Methods

Antibody and Reagents. Chemicals were from MilliporeSigma. Antibodies against IP6K1, IP6K2, IP6K3, myc tag (clone 9E10), flag tag (clone M2), GST, and vinculin were purchased from MilliporeSigma. Antibodies against DIC2, DLIC1, and p150glued were purchased from Bethyl Laboratories. Antibodies against cadherin, α-tubulin, phosphoserine/threonine, GFAP, β-actin, FAK, paxillin, phospho-FAK (Y397), phospho-FAK (Y576/577), phospho-FAK (Y925), and phosphopaxillin were purchased from Cell Signaling Technology. Antibodies against pericentrin, Satb2, and Ctip2 were from Abcam. Antibodies against calbindin, DHC, DIC1, DLC1/2, phosphotyrosine, HSP60, ACBD3, and normal rabit IgG were from Santa Cruz Biotechnology. Rhodamine phalloidin, Alexa Fluor 488 goat anti-rabbit, Alexa Fluor 568 goat anti-mouse IgG, and EdU were from Thermo Fisher Scientific. Anti LAMP1 antibody was from PhosphoSolutions.

Cell Culture. HEK 293 cells, HEK 293T cells, human neuroblastoma SH-SY5Y cells, *IP6K3* WT and KO MEF cells and astrocytes were cultured in DMEM supplemented with 10% (vol/vol) FBS, 100 units/mL penicillin and 100 μg/mL streptomycin. *IP6K3* WT and KO primary cortical neuronal cells were cultured in neurobasal-A medium (no glucose, no sodium pyruvate) supplemented with 12.5 mM glucose, 2 mM L-glutamine, and 2% (vol/vol)

B-27 supplement (minus antioxidants). Cell culture plates were coated with poly-L-ornithine for astrocytes and cortical neuronal cells. DIC2 knockdown SH-SY5Y cells were generated by lentiviral transduction. Virus-infected cells were selected using puromycin (5 μg/mL). All cells were maintained at 37 °C with 5% CO_2.

Animals. The *IP6K3* WT and KO animals were littermates from heterozygous breeding. Animal breeding and procedures were conducted in strict accordance with the NIH *Guide for Care and Use of Laboratory Animals* (58). Animal experiments were approved by the Johns Hopkins University Animal Care and Use Committee.

Western Blot and Immunoprecipitation. The lysis buffer contained 50 mmol/L Tris·HCl (pH 7.4), 100 mmol/L NaCl, 0.5% Igepal CA630, 5 mmol/L $MgCl_2$, protease inhibitors, and phosphatase inhibitors. Cells were lysed on ice, and the lysates were passed 20 times through a 30-gauge needle with syringe. The cell lysates were then centrifuged at 13,000 × *g* for 10 min at 4 °C. The supernatants were collected. Protein concentrations were determined by using Pierce BCA protein assay kit (Thermo Fisher Scientific) and equalized. Equal amounts of whole cell lysates were precleared with protein A/G agarose (Santa Cruz Biotechnology) for 1 h at 4 °C. Then the supernatants were added with antibody and incubated overnight at 4 °C followed by protein A/G agarose precipitation.

Immunofluorescence Staining. Animals were perfused and fixed with 4% paraformaldehyde (wt/vol). The brain slices were cut at 30-μm thickness. Cultured cells were washed with PBS and fixed with 4% paraformaldehyde (wt/vol). Slides were blocked with 10% goat serum (vol/vol) for 10 min at room temperature, followed by incubation with primary antibody at 4 °C overnight, and then, fluorescence-labeled secondary antibody for 1 h at room temperature. Cell nuclei were stained with DAPI. Slides were mounted with ProLong Gold antifade mountant. Pictures were taken with a confocal microscope (Zeiss LSM 700, National Institutes of Health Award No. S10 OD016374) or Nikon Eclipse Ti-ETIRF microscope.

RNA Isolation and PCR. Total RNA was isolated from brain tissues and cells using the RNeasy mini kit (Qiagen) and reverse transcribed to cDNA using SuperScript III (Invitrogen). PCR was run by using Titanium Taq DNA polymerase (Clontech). Primers are mouse IP6K1 forward: ATGTGTGTTTGTCAAACCATGGAAGT, reverse: CTACTGGTTCTCATCCCGCATCTGCT; mouse IP6K2 forward: ATGAGCCCAGCCTTCAGGACCATGGA, reverse: TCACTCCCCACTCTCCTCACTTATCTCT; mouse IP6K3 forward: ATGGTGGTGCGGCACAGCTCGGACAA, reverse: TCATTCTCCTTCCTGGATATCCCGCAGAAT; human IP6K1 forward: ATGTGTGTTTGTCAAACCATGGAAGT, reverse: CTACTGGTTCTCGTCCCGCATCTGTT; human IP6K2 forward: ATGAGCCCAGCCTTCAGGGCCATGGAT, reverse: TCACTCCCCACTCTCCTCACTTATCTCT; and human IP6K3 forward: ATGGTTGTGCAAAACAGCGCAGACGCCGGGGACAT, reverse: TCATTCTCCCTCTTGGATATCCTGCAGGAT.

Wound-Induced Migration Assay. For the wound-induced migration assay, a scratch wound was drawn on a confluent monolayer of cells. Cells were fixed 8 h later by 4% (wt/vol) paraformaldehyde and immunofluorescence staining was performed.

Subcellular Fractionation. The cytosol and nuclear fractions were isolated using the NE-PER nuclear and cytoplasmic extraction reagents (Thermo Fisher Scientific).

EdU Labeling of Neuronal Migration. Heterozygous breeding pregnant mice at E15.5 were injected i.p. with 100 mg/kg EdU in normal saline and fetuses were harvested at 24 or 48 h after injection. The fetuses were fixed with 4% (wt/vol) paraformaldehyde and cut as sagittal sections. The slices were stained with Alexa Fluor 488 PicolylAzide to label EdU-incorporated cells (Thermo Fisher Scientific).

In Vitro Protein Expression and Purification. The myc-tag GFP, myc-tag WT IP6K3, and myc-tag kinase-dead mutant IP6K3 were cloned into the pGEX-6P-2 vector (GE Healthcare Life Sciences). PreScission Protease was used to remove the GST from myc-tag GFP, myc-tag WT, and mutant IP6K3. GFP and DIC2 were also cloned into the pGEX-6P-2 vector (GE Healthcare Life Sciences) to produce GST-fused GFP and GST-fused DIC2.

Plasmid and Lentiviral Expression. The DIC2 shRNA and scrambled control plasmids were from MilliporeSigma. The myc-tagged GFP and myc-tagged human DIC2 were cloned to pCDH-EF1-MCS-T2A-copGFP vector (System Biosciences). The flag-tagged GFP and flag-tagged human WT IP6K3 constructs were cloned to pLVX-AcGFP1-N1 vector (Clontech). The flag-tagged IP6K3 fragments were cloned to pLVX-AcGFP1-N1 vector (Clontech). The myc-tagged murine WT and kinase-deficient (KD) IP6K3 were cloned to pCDH-EF1-MCS-T2A-copGFP vectors (System Biosciences). Lentivirus was generated by transfection of lentiviral vector together with pMD2.G and psPAX2 in HEK 293T cells (59).

Intracellular Inositol Phosphate Calculation. WT and *IP6K3* KO astrocytes were cultured in DMEM supplemented with 10% FBS, sodium pyruvate (Thermo Fisher Scientific) and GlutaMAX supplement (Thermo Fisher Scientific). The cell culture plates were coated with collagen. Cells were plated at 70% confluence and 100 μCi [^{3}H] myo-inositol was added to the medium and cultured for 3 d. The inositol phosphates were separated by HPLC (58).

Statistical Analysis. Quantitative data are expressed as means ± SEM. Data were analyzed by one-way ANOVA, unpaired Student's *t* test. $P < 0.05$ was considered statistically significant. For nonquantitative data, results were representative of at least three independent experiments.

ACKNOWLEDGMENTS. We thank Dr. Rashna Bhandari for discussions. This work was supported by US Public Health Service Grant MH18501 (to S.H.S.). Z.G., X.L., Y.W., and C.F. were supported by startup funding from Tianjin Medical University (to C.F.).

1. Chakraborty A (2018) The inositol pyrophosphate pathway in health and diseases. *Biol Rev Camb Philos Soc* 93:1203–1227.
2. Shears SB, Baughman BM, Gu C, Nair VS, Wang H (2017) The significance of the 1-kinase/1-phosphatase activities of the PPIP5K family. *Adv Biol Regul* 63:98–106.
3. Shears SB (2016) Towards pharmacological intervention in inositol pyrophosphate signalling. *Biochem Soc Trans* 44:191–196.
4. Illies C, et al. (2007) Requirement of inositol pyrophosphates for full exocytotic capacity in pancreatic beta cells. *Science* 318:1299–1302.
5. Rajasekaran SS, et al. (2018) Inositol hexakisphosphate kinase 1 is a metabolic sensor in pancreatic β-cells. *Cell Signal* 46:120–128.
6. Saiardi A, Bhandari R, Resnick AC, Snowman AM, Snyder SH (2004) Phosphorylation of proteins by inositol pyrophosphates. *Science* 306:2101–2105.
7. Gu C, et al. (2017) KO of 5-InsP$_7$ kinase activity transforms the HCT116 colon cancer cell line into a hypermetabolic, growth-inhibited phenotype. *Proc Natl Acad Sci USA* 114:11968–11973.
8. Zhu Q, et al. (2016) Adipocyte-specific deletion of Ip6k1 reduces diet-induced obesity by enhancing AMPK-mediated thermogenesis. *J Clin Invest* 126:4273–4288.
9. Burton A, Azevedo C, Andreassi C, Riccio A, Saiardi A (2013) Inositol pyrophosphates regulate JMJD2C-dependent histone demethylation. *Proc Natl Acad Sci USA* 110: 18970–18975.
10. Hou Q, et al. (2018) Inhibition of IP6K1 suppresses neutrophil-mediated pulmonary damage in bacterial pneumonia. *Sci Transl Med* 10:eaal4045.
11. Malla AB, Bhandari R (2017) IP6K1 is essential for chromatoid body formation and temporal regulation of *Tnp2* and *Prm2* expression in mouse spermatids. *J Cell Sci* 130: 2854–2866.
12. Fu C, et al. (2018) Multiple aspects of male germ cell development and interactions with Sertoli cells require inositol hexakisphosphate kinase-1. *Sci Rep* 8:7039.
13. Morrison BH, et al. (2009) Gene deletion of inositol hexakisphosphate kinase 2 predisposes to aerodigestive tract carcinoma. *Oncogene* 28:2383–2392.
14. Morrison BH, et al. (2002) Inositol hexakisphosphate kinase 2 sensitizes ovarian carcinoma cells to multiple cancer therapeutics. *Oncogene* 21:1882–1889.
15. Rao F, et al. (2014) Inositol pyrophosphates mediate the DNA-PK/ATM-p53 cell death pathway by regulating CK2 phosphorylation of Tti1/Tel2. *Mol Cell* 54:119–132.
16. Fu C, et al. (2015) Inositol hexakisphosphate kinase-3 regulates the morphology and synapse formation of cerebellar purkinje cells via spectrin/adducin. *J Neurosci* 35: 11056–11067.
17. Moritoh Y, et al. (2016) Inositol hexakisphosphate kinase 3 regulates metabolism and lifespan in mice. *Sci Rep* 6:32072.
18. Crocco P, et al. (2016) Contribution of polymorphic variation of inositol hexakisphosphate kinase 3 (IP6K3) gene promoter to the susceptibility to late onset Alzheimer's disease. *Biochim Biophys Acta* 1862:1766–1773.
19. Vallee RB, McKenney RJ, Ori-McKenney KM (2012) Multiple modes of cytoplasmic dynein regulation. *Nat Cell Biol* 14:224–230.
20. Reck-Peterson SL, Redwine WB, Vale RD, Carter AP (2018) The cytoplasmic dynein transport machinery and its many cargoes. *Nat Rev Mol Cell Biol* 19:382–398.
21. Siglin AE, et al. (2013) Dynein and dynactin leverage their bivalent character to form a high-affinity interaction. *PLoS One* 8:e59453.
22. Schroer TA (2004) Dynactin. *Annu Rev Cell Dev Biol* 20:759–779.
23. Dujardin DL, et al. (2003) A role for cytoplasmic dynein and LIS1 in directed cell movement. *J Cell Biol* 163:1205–1211.

24. Tsai JW, Bremner KH, Vallee RB (2007) Dual subcellular roles for LIS1 and dynein in radial neuronal migration in live brain tissue. *Nat Neurosci* 10:970–979.
25. Tsai JW, Lian WN, Kemal S, Kriegstein AR, Vallee RB (2010) Kinesin 3 and cytoplasmic dynein mediate interkinetic nuclear migration in neural stem cells. *Nat Neurosci* 13: 1463–1471.
26. Folker ES, Schulman VK, Baylies MK (2014) Translocating myonuclei have distinct leading and lagging edges that require kinesin and dynein. *Development* 141: 355–366.
27. Grabham PW, Seale GE, Bennecib M, Goldberg DJ, Vallee RB (2007) Cytoplasmic dynein and LIS1 are required for microtubule advance during growth cone remodeling and fast axonal outgrowth. *J Neurosci* 27:5823–5834.
28. Laan L, et al. (2012) Cortical dynein controls microtubule dynamics to generate pulling forces that position microtubule asters. *Cell* 148:502–514.
29. Geiger B, Spatz JP, Bershadsky AD (2009) Environmental sensing through focal adhesions. *Nat Rev Mol Cell Biol* 10:21–33.
30. Broussard JA, Webb DJ, Kaverina I (2008) Asymmetric focal adhesion disassembly in motile cells. *Curr Opin Cell Biol* 20:85–90.
31. Wu Y, et al. (2016) In-situ coupling between kinase activities and protein dynamics within single focal adhesions. *Sci Rep* 6:29377.
32. Zaidel-Bar R, Milo R, Kam Z, Geiger B (2007) A paxillin tyrosine phosphorylation switch regulates the assembly and form of cell-matrix adhesions. *J Cell Sci* 120: 137–148.
33. Webb DJ, et al. (2004) FAK-Src signalling through paxillin, ERK and MLCK regulates adhesion disassembly. *Nat Cell Biol* 6:154–161.
34. Ilić D, et al. (1995) Reduced cell motility and enhanced focal adhesion contact formation in cells from FAK-deficient mice. *Nature* 377:539–544.
35. Yu DH, Qu CK, Henegariu O, Lu X, Feng GS (1998) Protein-tyrosine phosphatase Shp-2 regulates cell spreading, migration, and focal adhesion. *J Biol Chem* 273: 21125–21131.
36. Angers-Loustau A, et al. (1999) Protein tyrosine phosphatase-PEST regulates focal adhesion disassembly, migration, and cytokinesis in fibroblasts. *J Cell Biol* 144: 1019–1031.
37. McWilliam H, et al. (2013) Analysis tool web services from the EMBL-EBI. *Nucleic Acids Res* 41:W597–W600.
38. Chanduri M, et al. (2016) Inositol hexakisphosphate kinase 1 (IP6K1) activity is required for cytoplasmic dynein-driven transport. *Biochem J* 473:3031–3047.
39. Steffen W, et al. (1997) The involvement of the intermediate chain of cytoplasmic dynein in binding the motor complex to membranous organelles of Xenopus oocytes. *Mol Biol Cell* 8:2077–2088.
40. Duellberg C, et al. (2014) Reconstitution of a hierarchical +TIP interaction network controlling microtubule end tracking of dynein. *Nat Cell Biol* 16:804–811.
41. Manneville JB, Jehanno M, Etienne-Manneville S (2010) Dlg1 binds GKAP to control dynein association with microtubules, centrosome positioning, and cell polarity. *J Cell Biol* 191:585–598.
42. Fu C, et al. (2017) Neuronal migration is mediated by inositol hexakisphosphate kinase 1 via α-actinin and focal adhesion kinase. *Proc Natl Acad Sci USA* 114:2036–2041.
43. Jadav RS, et al. (2016) Deletion of inositol hexakisphosphate kinase 1 (IP6K1) reduces cell migration and invasion, conferring protection from aerodigestive tract carcinoma in mice. *Cell Signal* 28:1124–1136.
44. Pasapera AM, Schneider IC, Rericha E, Schlaepfer DD, Waterman CM (2010) Myosin II activity regulates vinculin recruitment to focal adhesions through FAK-mediated paxillin phosphorylation. *J Cell Biol* 188:877–890.
45. Rao F, et al. (2015) Inositol pyrophosphates promote tumor growth and metastasis by antagonizing liver kinase B1. *Proc Natl Acad Sci USA* 112:1773–1778.
46. Chakraborty A, et al. (2010) Inositol pyrophosphates inhibit Akt signaling, thereby regulating insulin sensitivity and weight gain. *Cell* 143:897–910.
47. Matanis T, et al. (2002) Bicaudal-D regulates COPI-independent Golgi-ER transport by recruiting the dynein-dynactin motor complex. *Nat Cell Biol* 4:986–992.
48. Tan SC, Scherer J, Vallee RB (2011) Recruitment of dynein to late endosomes and lysosomes through light intermediate chains. *Mol Biol Cell* 22:467–477.
49. Shu T, et al. (2004) Ndel1 operates in a common pathway with LIS1 and cytoplasmic dynein to regulate cortical neuronal positioning. *Neuron* 44:263–277.
50. Cianfrocco MA, DeSantis ME, Leschziner AE, Reck-Peterson SL (2015) Mechanism and regulation of cytoplasmic dynein. *Annu Rev Cell Dev Biol* 31:83–108.
51. Ligon LA, Karki S, Tokito M, Holzbaur EL (2001) Dynein binds to beta-catenin and may tether microtubules at adherens junctions. *Nat Cell Biol* 3:913–917.
52. Rosse C, et al. (2012) Binding of dynein intermediate chain 2 to paxillin controls focal adhesion dynamics and migration. *J Cell Sci* 125:3733–3738.
53. Park AY, Shen TL, Chien S, Guan JL (2009) Role of focal adhesion kinase Ser-732 phosphorylation in centrosome function during mitosis. *J Biol Chem* 284: 9418–9425.
54. Xie Z, Sanada K, Samuels BA, Shih H, Tsai LH (2003) Serine 732 phosphorylation of FAK by Cdk5 is important for microtubule organization, nuclear movement, and neuronal migration. *Cell* 114:469–482.
55. Hafezparast M, et al. (2003) Mutations in dynein link motor neuron degeneration to defects in retrograde transport. *Science* 300:808–812.
56. Schlomann U, Schwamborn JC, Müller M, Fässler R, Püschel AW (2009) The stimulation of dendrite growth by Sema3A requires integrin engagement and focal adhesion kinase. *J Cell Sci* 122:2034–2042.
57. LaMonte BH, et al. (2002) Disruption of dynein/dynactin inhibits axonal transport in motor neurons causing late-onset progressive degeneration. *Neuron* 34:715–727.
58. National Research Council (2011) *Guide for the Care and Use of Laboratory Animals* (National Academies Press, Washington, DC), 8th Ed.
59. Fu C, et al. (2018) Inositol polyphosphate multikinase inhibits angiogenesis via inositol pentakisphosphate-induced HIF-1α degradation. *Circ Res* 122:457–472.